Aerodynamic Analysis of Spiral Grooved Thrust Bearing

Project Report Submitted to
National Institute of Technology, Rourkela
For the partial fulfilment of the requirement
of
Master of Technology
in
Mechanical Engineering
by

Chitranjan Kumar
(Roll No: 214ME1544)

Under the guidance
of
Prof. Suraj Kumar Behera

DEPARTMENT OF MECHANICAL ENGINEERING
NATIONAL INSTITUTE OF TECHNOLOGY, ROURKELA
MAY-2016

Mechanical Engineering
National Institute of Technology Rourkela

Prof. Suraj Kumar Behera

Assistant Professor

May 2016

Supervisor's Certificate

This is to certify that the work presented in this dissertation entitled '*Aerodynamic Analysis of Spiral Grooved Thrust bearing*' by "*Chitranjan Kumar''*, Roll Number 214ME1544, is a record of original research carried out by him/her under my supervision and guidance in partial fulfillment of the requirements of the degree of *Master of Technology* in *Mechanical Engineering*. Neither this dissertation nor any part of it has been submitted for any degree or diploma to any institute or university in India or abroad.

Suraj Kumar Behera

Declaration of Originality

I, *Chitranjan Kumar,* Roll Number *214ME1544* hereby declare that this dissertation entitled "*Aerodynamic Analysis of Spiral Grooved Gas Thrust Bearing"* represents my original work carried out as a postgraduate student of NIT Rourkela and, to the best of my knowledge, it contains no material previously published or written by another person, nor any material presented for the award of any other degree or diploma of NIT Rourkela or any other institution. Any contribution made to this research by others, with whom I have worked at NIT Rourkela or elsewhere, is explicitly acknowledged in the dissertation. Works of other authors cited in this dissertation have been duly acknowledged under the section "Bibliography". I have also submitted my original research records to the scrutiny committee for evaluation of my dissertation.

I am fully aware that in case of any non-compliance detected in future, the Senate of NIT Rourkela may withdraw the degree awarded to me on the basis of the present dissertation.

May 2016

NIT, Rourkela Chitranjan Kumar

Acknowledgment

At first I would like to thanks the director, Pof. S K Sarangi, of our institute NIT, Rourkela for providing the wonderful reading atmosphere in the institute. I also like to thank our Head of Department, Prof. S S Mohapatra sir for making all the facilities available in the department updated.

Now I would like to thank my guide Prof. Suraj Kumar Bahera sir for his support throughout the project duration. It was not possible to make this effort fruitful without his support.

I also like to thank all my lab mates with whom I have discusses the problem and got the right solution as soon as possible.

At last I would like to thank all my RSS brothers of Aryabhat Sakha NIT, Rourkela for making my stay here as one of the memorable part of my life.

Abstract

Thrust bearings are designed to support the axial loads generated by the rotating component of turbomachinary like turbocharger and turboexpander. Aerodynamic gas thrust bearing like tilting pad, tapered pad, grooved has been successfully designed and developed. Previously it was difficult and costly to generate spiral grooves but now it easily be developed with laser machining process. Current research target to design and develop an alternative aerodynamic grooved thrust bearing with spiral pattern to find pressure profile, load carrying capacity and friction coefficient etc. In this analysis Reynolds Equation is solved by using the Finite Difference Method (FDM) to get the pressure distribution over the surface of the spiral grooved bearing. After the pressure distribution is known, load carrying capacity and friction coefficient is calculated and their variation with different parameters are presented. The suitability of designed bearing is checked for the designed turbocharger. Here the resultant axial thrust load is calculated for the designed micro turbocharger and this axial thrust load is compared with the load carrying capacity of the designed bearing. The author believe that the detail and procedural analysis will help the researchers to design and develop more alternative gas bearing for micromachinary like turbocharger and turboexpander etc.

Keywords: - Turbocharger, FDM, Thrust Bearing

Contents

List of Figures

Nomenclature

1.	$F_{1,C}$	The pressure force acting on the inlet surface.
2.	$F_{2,C}$	The pressure force at the shroud surface.
3.	$F_{3,C}$	The impulsive force acting on the CW
4.	$F_{4,C}$	The pressure force at the back face of CW
5.	$F_{1,T}$	The pressure force acting on the inlet surface.
6.	$F_{2,T}$	The pressure force at the shroud surface
7.	$F_{3,T}$	The impulsive force acting on the TW
8.	$F_{4,T}$	The pressure force at the back face of TW
9.	D_1	Inflow diameter of the compressor (mm)
10.	A_{in}	Inlet cross-sectional area of the CW
11.	p_1	Inlet pressure of the atmospheric air (Pa)
12.	p_2^*	Outlet pressure of the CW
13.	b_1	Blade height at inlet (mm)
14.	b_2	Blade height at inlet (mm)
15.	D_2	Outlet diameter of the compressor (mm)
16.	z	Number of blades
17.	t	The blade thickness (mm)
18.	p_2	Outlet pressure of the diffuser (Pa)
19.	r_C	The reaction degree of the compressor
20.	T_1	Inlet temperature inlet temperature (K)
21.	$\rho_{in,c}$	Inlet density (Kgm-3)
22.	$A_{S,C}$	Projected area in the axial direction (here along x-direction) of the shroud surface
23.	N	RPM of the CW
24.	$\dot{m}_C$	Mas flow rate of air through CW

25.	$C_{m,1}$	Meridional component of the air velocity at compressor inlet
26.	R_a	Characteristic gas constant foe air ($Jkg^{-1}K^{-1}$)
27.	F_{CW}	Resultant force acting on the CW (N)
28.	p_3	The pressure of air in the vane less space of the turbine (Pa)
29.	p_4	The pressure at the outlet of the turbine (Pa)
30.	D_3	Inlet diameter of the turbine (mm)
31.	D_4	Outlet diameter of the turbine (mm)
32.	b_3	Blade height at inlet (mm)
33.	b_4	Outlet blade height (mm)
34.	D_{tip}	Diameter of the turbine tip (mm)
35.	D_{hub}	Diameter of the turbine hub (mm)
36.	z	Number of turbine blades
37.	t	Blade thickness of the turbine (mm)
38.	T_3	Inlet temperature of the turbine (K)
39.	$\rho_{in,T}$	Inlet density of the turbine (Kgm-3)
40.	$A_{bf,T}$	Back face surface area of the TW
41.	F_{TW}	Resultant force acting on the TW (N)
42.	$F_{T,ax}$	Resultant axial-thrust force acting on the Rotor (N)
43.	r_i	Inlet radius of the bearing
44.	r_o	Outer radius of the bearing
45.	α	Spiral Angle (degree)
46.	TG	Groove Angle (degree)
47.	TL	Land Angle (degree)
48.	p_{at}	Atmospheric pressure (Pa)
49.	h	Film thickness (m)
50.	μ	Kinematic viscosity of air (Pa-s)
51.	ω	Angular Velocity (rad/s)
52.	$\wedge$	Bearing number

Chapter-1

Introduction

1.1 Basics of Spiral Grooved Bearing

Rotor-bearing system is an essential part in most of the micro turbo machines whose stability of functioning increases the efficiency of the machine. The stability of a journal bearing depends upon several factors among which eccentricity is the most vital one. The low eccentric figure associated with poor stability of the journal bearings and its stability enhances with the gradual rise in the value of eccentricity. In the working of Turbo machinery in general, the power loss, frequency and the vibration amplitudes are the major parameters of efficiency which mostly depends upon the nature of bearings used in the machine along with some other factors. Therefore, it is very much important to discuss the stability of journal bearings.

Plain journal bearings are inexpensive and easy in manufacturing but, it suffers with poor stability due to its low eccentricity. In order to improve the stability the journal was pre-loaded by designing a geometrical shape in it such as dams, pockets, steps etc. In the as such design of plain journal bearings the lubricants present inside the geometrical shape creates some additional loads before running of the rotor and hence these additional loads are able to increase the stability of the rotor-bearing systems.

Tilting pad journal bearing is also able to provide more stability to the rotor-bearing systems however; its design is much more complex in nature.

In this context the discussion on spiral groove bearing or helical groove bearings are much more important as they are now widely used in micro machines as thrust journal bearings.

Spiral grooved bearing is one among the many successful attempt which are mostly used as thrust bearing in micro machines in which gas, grease or oil are used as lubricants. Spiral groove bearings are designed by cutting some shallow grooves either on the surface of the journal or on the bearing surface. There is some leaning of the groves with respect to the rotational direction of the rotor or journal. This angle of inclination is known as groove angle. This designed grooves enable automatic pumping of lubricants into the spiral grooves due to which additional pressure is generated inside the bearing. This generated pressure reloads the bearing which increases the rotor stability. The spiral groove bearing performance depends on

groove depth, groove width, groove angle, and grooves number on bearing surface. There are several types of spiral groove thrust bearings. However, we will explain only three important ones such as: -

I. Symmetrical spiral groove bearing.
II. Asymmetrical spiral groove bearing and
III. Partially grooved bearing.

Symmetrical spiral groove thrust bearing are those in which all the designed grooves are of equal length about the mid axial plane of the bearing but spiral angle is in opposite to the rotor rotational directions. Here, due to rotation of the rotor the lubricant is pumped towards the centre of the bearing and there is no lubricant net flow of takes place out of the bearing except some leakage flow.

In the asymmetrical spiral grooved thrust bearing, the grooves length on one side of the bearing are marginally longer than those on the other side and therefore, a resultant axial flow of lubricant takes place inside it. In the partially grooved bearing, grooving is done only on half of the bearing surface and the remaining half is left plain.

Similar to Asymmetrical bearing, resultant axial flow of lubricant also takes place in partially grooved thrust bearings. A large part of thermal energy generated during friction is dissipated by the outward flow of lubricants and hence the ability of pumping keeps much importance in these bearings.

1.2 Objective of the Present Work

The main objective of the present work was to design a spiral grooved thrust bearing which can be used to support the rotor of a designed turbo expander.

In order to fulfil the desired objective, net generated thrust load for the designed turbo expander was calculated. Depending on the above calculated data a spiral grooved thrust bearing was designed. All the calculations and results of present work are explain in the different chapters as below.

Chapter-2 is dedicated to the Literature review. In chapter-3, the resultant thrust load generated in the designed turbo expander is calculated. Chapter-4 explains about the mathematical formulation of the governing equation and it also explains about the FDM followed in order to solve the Reynolds equation. The spiral grooved thrust bearing characteristics are analysed and presented in chapter-5. Lastly, conclusion and future work recommendation are mentioned in chapter-6 and the chapter-7 is dedicated to references.

Chapter 2: Literature Review

In general we use the Reynolds equation to derive the pressure distribution of lubricated film in all type of bearings. In the case of spiral groove bearing the profile of pressure along the circumferential direction is of saw tooth shape.

It was Wipple [1] who successfully described the working of a spiral groove bearing by applying basic hydrodynamics theory. He however, considered the assumptions similar to that of analysing the smooth bearings like plain journal bearings.

Again it was Muijderman [2] who also successfully tried to solve the problems related to the lubricated spiral groove bearing. He assumed different initial parameters to analyse the bearing's load carrying capacity as well as power losses due to frictions. He had also reported the effect of groove parameters on the working performance of the bearing

However, it was Vohr and Chow [3] and separately by Hirs [4] who successfully forwarded a theoretical model to apply the Reynolds equation to spiral groove bearing for the first time and derived the required solutions for such bearings. They proposed that actual pressure profile is not needed always to find the load carrying capacity and stability of the spiral grooved bearing, instead, it is sufficient to identify the mean pressure across the width of a groove and land pair. According to them this proposed pressure profile is known as a smoothed pressure profile, is applicable only when there is infinite number of grooves either on the surface of the bearing or on the surface of the journal. But in real life it is not possible to generate infinite number of grooves either on the surface of a journal or on the surface of a bearing. Though, the proposed theoretical analysis is quite accurate when it is applied to bearings having finite number of grooves.

It was Hirs and Bootsma [5] who verified this proposed theory experimentally and opened the door for further study in this direction.

In another approach of finite difference method, Smally [6] solved the differential equation for the smoothed pressure profile. They assumed that the lubricant viscosity remains constant across the film. Basing upon this assumption they found results which were very close to the experimental one. On the other hand, Reinhoudt [7] used the method of finite element analysis to solve the problems related to the helical grooved bearings. In an extensive approach it was Yavelo [8] who tried to increase the load carrying capacity of a spiral groove bearing by optimizing several affecting parameters of the grooves.

It was Cunning and Fleming [9] who carried out an experimental stability analysis of the gas lubricated herringbone bearing. They were successfully attained a speed of 60000rpm without

the application of any radial load with perfect stability. In addition they also found that the stability can be improved by reducing the bearing clearance.

Malanoski [10] also reported of attaining a speed of 60000 rpm without instability in an ultra-stable gas bearing of 40mm diameter and loaded eccentricity of 0.3.

Again, Molyneaux [11] also reported a stainless steel rotor running at a speed of 350000 rpm used in a 9mm spiral groove journal bearing which is suitably applied in industries. It is also reported that for the working of an expansion turbine helical groove journal bearing is used to support a rotor.

It is observed that in an air lubricated spiral groove bearings the load carrying capacity are too small for most engineering applications. Therefore, it is very much important to increase the load carrying capacity of the bearing for which a high viscous substance should substitute air as a lubricant in the bearings. Grease as a lubricant can be a suitable alternative for air where a self-sealing action for the bearing is required. Dewar [12] and Muijdeman [13] have explained theoretically as well as experimentally the application of Grease as lubricant in spiral grooved bearing.

Apart from this Fredrick [14] conducted some experiments taking sodium as lubricant. They have chosen four different journals bearing varying in groove nature and conducted their experiment within a temperature range of 500 °F to 800 °F, maintained the diameter of the bearings as 40mm and speed to 12000rpm. From the above experiments, they concluded that the tilting pad bearing is the most stable followed by the plain journal bearing with a herringbone grooved journal. However, the stability of the axial groove bearing is the least. In a separate experiment carried by them taking water as lubricant they observed that the stability of the rotor was not affected by the number of grooves present in the journal.

A theoretical investigation on turbulent flow journal bearing was carried out by Vohr and Chow [15]. They have chosen spiral grooves of different configurations to know the effect of nature of mounting of grooving. For an incompressible lubricant they observed that the mounting of grooving whether on the surface of journal or on the surface of bearing has no significant effect on the performance of the rotor bearing system.

First time it was Bootsma [16] who investigated the effect of lubricant on the performance of the bearing whose viscosity varies with different parameters. The application of spiral groove bearing as a supportive part to the milling machine was studied by Yavelov [17]. Nobuyoshi and Yashumi [18] have studied the performance of a spiral groove bearing using reversible herringbone journal bearing. Their theoretical investigation found that the load bearing

capacity of reversible herring bone journal bearing is comparatively smaller than the conventional type.

There are two different methods to generate grooves either on the bearing surface or on the surface of a journal. The first one is the chemical etching process which is explained by Hirs [19]. The second one is the generation of grooves over the surface by milling.

Yuan Huang and Di-Gong Chen [20] are followed the perturbation method to investigate the effect of partial grooving on the performance of the spiral grooved spherical and conical bearing. They concluded that the load carrying capacity and stiffness of the bearing was not significantly affected by the partial grooving as long as partial-grooving ratio (PGR) is below 0.2.

Liu Ren and Wang Xiaoli [21] had studied about the effect of structural parameters like groove depth ratio, spiral angle, groove angle, land angle etc., on the behaviours of micro spiral-grooved thrust bearing. They explored the optimum structural parameters of the spiral grooved bearing and presented the result in terms of maximum non-dimensional load carrying capacity.

Ren Liu et al., [22] had investigated the dynamic characteristics of the spiral grooved thrust bearing having slip-flow. They also investigated the effects of gas rarefaction on the dynamic characteristics of the spiral-grooved thrust bearing.

Huang, J. B et al., [23] proposed a design for the fabrication of a micro hydrodynamic thrust bearing. They also discussed about the different issues related to scaling of the design.

Wong, C. W. et al., [24] explain the design, fabrication and testing of a self-acting grooved thrust bearing which was integrated in a high-speed micro turbine.

Grigor'ev, B. S., & Smirnov, D. B. [25] were followed a numerical method and solve the Reynolds equation by finite element analysis to know the characteristics of the gas-lubricated thrust bearing. All the design parameters were optimised on the basis of load carrying capacity w.r.t. the number of grooves and the compressibility number.

Wang, B., et al., [26] were numerically obtained the turbulent field of a spiral-grooved dry-gas seal to know the effect of turbulence on the seal performance. They sued the Direct Numerical Simulation and Reynolds-averaged Navier- Stokes (RANS) method to know the velocity field properties in the lubricant film. They calculated the forces acting on the sealed by integrating the pressure distribution.

Šimek, J., & Lindovský, P. [27] were designed, manufactured and tested an aerodynamic bearing support having operating speed up to 65000 rpm. Different characteristics variation like stiffness, damping with speed were presented.

Villavicencio, R. et al., [28] were experimentally tested a micro thrust bearing used in a high speed compressor to generate electricity in a vehicle using fuel cell system. They were tested the designed bearing with a test bench at 100000 rpm in stable rotational speed. They were done the comparison between the spiral grooved and taper land thrust bearing and find that they have good correlation between them.

Muhammad Zubair Khan [29] had done the experimental as well as theoretical analysis of different types of spiral grooved journal bearings. He had calculated the load carrying capacity, stiffness and damping and stability characteristics of different types of spiral grooved bearings. From both, theoretical and experimental, results shows that at low load carrying capacity the spiral grooved bearings are more stable especially when the eccentricity ratio is low. On the other hand he also found that partial grooved spiral grooved journal bearing is suitable in practical life due to its misalignment behaviour above certain load.

Chapter-3

Thrust Load Calculation

3.1 Thrust-Load Calculation of the Rotor

To design the thrust bearing used for the high speed turbomachinery, the thrust load calculation must be resolute. Thrust load is generated by different pressure acting upon the compressor and turbine wheels as well as the impulsive force generated due to the flow in axial direction. Since the turbomachinery operates at various speeds therefore the thrust load depends on the speed of the rotor.

There are generally two ways to calculate the thrust load on the rotor: either using the CFD (computational fluid dynamics) or by simply applying the Newton's second law. The CFD method gives the precise result but needs huge computational exertion at all stages of turbomachinery, while using the Newton's second law is quite simple but needed some thermodynamics and turbomachinery knowledge. Though it's analytical result is quite good as compared to the numerical result obtained by CFD. The result difference between both the methods is generally lower than the safety tolerance of the thrust load taken in the bearing design. Therefore the Newton's second law is applied to the control volume for the thrust load calculation on the rotor.

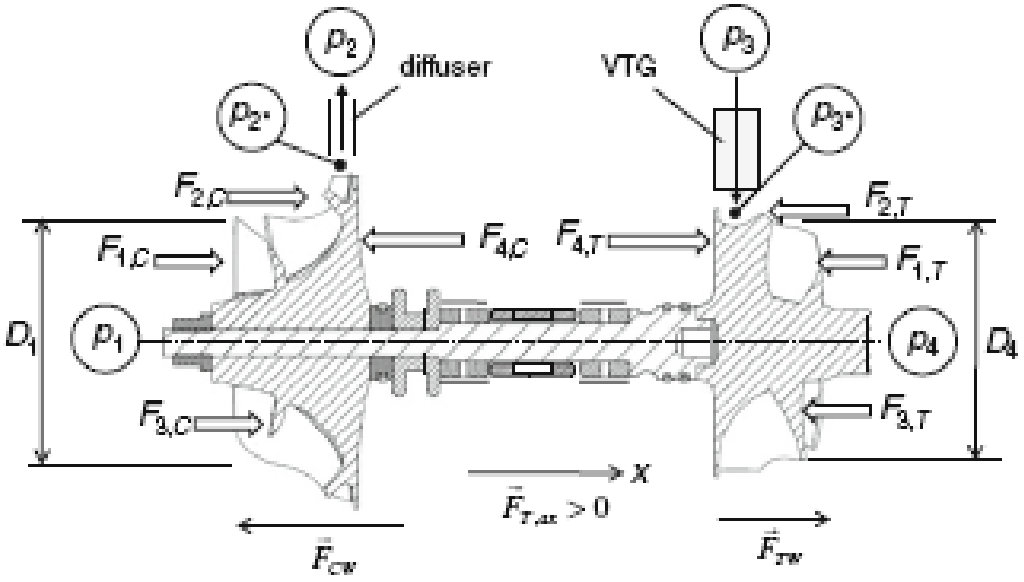

Figure 3.0:1: Forces acting on Turbocharger [30]

As the rotor is symmetric, the resultant force on the rotor acts along the axial direction (i.e., along x-direction), here it is represented as $F_{T,ax}$ (Fig.3.1).

The $F_{T,ax}$ is the resultant thrust load acting on the rotor, is the resultant of all forces acting on the compressor as well as turbine wheel as indicated in the Fig.3.1. Different forces acting on the compressor wheel (CW), which is in the left side of the diagram, $F_{1,C}$ is the pressure force acting on the inlet surface; $F_{2,C}$ is the pressure force at the shroud surface; $F_{3,C}$ is the impulsive force acting on the CW and $F_{4,C}$ is the pressure force at the back face of CW. Similarly, different forces acting on the turbine wheel (TW, in left portion of the Fig.3.1) can be represented as $F_{1,T}$, $F_{2,T}$, $F_{3,T}$ and $F_{4,T}$.

From reference [30] for D_1 =15mm and p_1 =1.01x10^5 Pa pressure force $F_{1,C}$ can be calculated by using the equation

$$F_{1,C} = A_1 p_1 = \frac{\pi D_1^2}{4} p_1 = 17.848N \quad \text{---------- (3.1)}$$

Where D_1 is the diameter of compressor at inlet

p_1 is the atmospheric air inlet pressure.

From the reference [30] for given value of blade height at inlet $b_1 = 3mm$ and at outlet $b_2 = 0.657mm$ one can calculate the mean blade height as

$$b_m = \frac{b_1 + b_2}{2} = 1.8285mm$$

Therefore the projected area of the shroud surface in the axial direction (here along X-direction) $A_{S,C}$ for given value of the outlet diameter of the compressor $D_2 = 33.7mm$, number of blades $z = 12$, and thickness of the blade $t = 0.75mm$ from the reference [30], can be calculated as

$$A_{S,C} = \frac{\pi\left(D_2^2 - D_1^2\right)}{4} - z \times b_m \times t = 6.9878 \times 10^{-4} m^2 \quad \text{---------- (3.2)}$$

The inlet and outlet pressure, temperature and fluid mass flow rate of the compressor cab be computed by using the turbomachinary processing. However, the value of the pressure p_2^* between the CW outlet and the diffuser are unknown. It is very difficult to calculate the above said pressures by means of measurement due to very narrow geometries of the gap between the

wheel and their housings. Therefore, it is estimated in terms of reaction degrees of the compressor.

The reaction degree r_C of the compressor is defined as the ratio of the enthalpy increase in the CW to the enthalpy increase in the compressor stage. The value of the reaction degree of the compressor is normally between 55 to 60% for all operating conditions and it can be expressed as

$$r_C = \frac{\Delta h_C}{\Delta h_{st}} = \frac{1-\left(\frac{P_2^*}{p_1}\right)^{\frac{k_a-1}{k_a}}}{1-\left(\frac{p_2}{p_1}\right)^{\frac{k_a-1}{k_a}}}$$

Where

k_a Is the isentropic exponent of the air for compressor (here $k_a = 1.4$ from reference [30]);

p_1 Is the atmospheric air inlet pressure to the CW

p_2 Is the outlet pressure of the diffuser (here $p_2 = 4.45\times10^5 Pa$ from reference [30]);

The value of r_C from reference [34] is taken as $r_C = 0.55$. By solving the above equation the p_2^* is given by

$$p_2^* = p_1\left[1+r_C\left(\left(\frac{p_2}{p_1}\right)^{\frac{k_a-1}{k_a}}-1\right)\right]^{\frac{k_a}{k_a-1}} = 2.9344\times10^5 Pa \qquad \text{---------- (3.3)}$$

The mean pressure of the compressor wheel on the basis of inlet pressure p_1 and the outlet pressure $p_2^* = 2.9344\times10^5 Pa$ can be calculated as

$$p_m = \left(\frac{p_1+p_2^*}{2}\right) = 1.9722\times10^5 Pa$$

By using the above calculated value of the mean pressure, we can calculate $F_{2,C}$ as follows

$$F_{2,C} = A_{S,C}\, p_m = A_{S,C}\left(\frac{p_1 + p_2^*}{2}\right) = 137.8161N \quad \text{---------- (3.4)}$$

Where

$A_{S,C}$ is the projected area of the shroud surface in the axial direction (here along x-direction);

p_1 is the CW inlet pressure;

p_2^* is the CW outlet pressure.

For the inlet pressure p_1, inlet temperature $T_1 = 300K$ and inlet density $\rho_{in,c} = 1.176kgm^{-3}$ the mass flow rate $\dot{m}_C$ can be calculated as

$$\dot{m}_c = \rho_{in,c} \times A_1\left(\frac{\pi \times D_1 \times N}{60}\right) = 0.0163kgs^{-1}$$

Where

N is the RPM of the CW.

For the given value of the RPM of CW, say N =100000rpm.

The impulsive force $F_{3,C}$ can be calculated by using the momentum theorem and the perfect gas equation as follows

$$F_{3,C} = \dot{m}_C\, C_{m,1} = \dot{m}_C\left(\frac{\dot{m}_C}{\rho_1 A_1}\right) = \frac{\dot{m}_C^{\,2} R_a T_1}{p_1 A_1} = 1.2854N \quad \text{---------- (3.5)}$$

Where

$\dot{m}_C$ is the mas flow rate of air through CW;

$C_{m,1}$ is the meridional component of the air velocity at compressor inlet;

R_a is the air characteristic gas constant;

T_1 is inlet temperature of air;

p_1 is the CW inlet pressure;

And A_{in} is cross-sectional area of the CW at the inlet.

According to the CFD result if the gap between bearing bushing and the back face of CW is more than 1mm then the pressure at the back face of CW is nearly remain unchanged. Hence, the pressure force $F_{4,C}$ corresponding to the pressure p_2^* can be calculated as

$$F_{4,C} = A_{bf,C} p_2^* = 90.0889N$$

Where

$A_{bf,C}$ is the CW back face surface area;

p_2^* is the CW outlet pressure.

The resulting force acting on the CW can be calculated as

$$F_{CW} = F_{1,C} + F_{2,C} + F_{3,C} - F_{4,C} = 66.8608N \quad \text{---------- (3.6)}$$

The inlet and outlet pressure, temperature and mass flow rate of the turbine cab be calculated by using the turbomachinary processing. Though, the value of the pressure p_3^* between the nozzle outlet and the vane less space of the turbine are unknown. It is very difficult to calculate the above said pressures by means of measurement due to very narrow geometries of the gap between the wheel and their housings. Hence, it is estimated in terms of reaction degrees of the turbine.

The reaction degree r_T of the turbine is defined as the ratio of the enthalpy decrease in the TW to the enthalpy decrease in the expansion stage. Where the reaction degree of the turbine is varied from 20% to 90% depending on the position of the west gate and it can be expressed as

$$r_T = \frac{\Delta h_T}{\Delta h_{St}} = \frac{1 - \left(\frac{p_4}{p_3^*}\right)^{\frac{k_g - 1}{k_g}}}{1 - \left(\frac{p_4}{p_3}\right)^{\frac{k_g - 1}{k_g}}}$$

Where

k_g = is the isentropic exponent of exhaust gas (from reference [30] $k_g = 1.32$)

p_3 is the pressure of air in the vane less space of the turbine

Here, the value of p_3 from reference [35] is $p_3 = 4.319 \times 10^5 Pa$

p_4 is the pressure at the outlet of the turbine (from reference [35] $p_4 = 1.02 \times 10^5 Pa$)

The above expression can be solved to calculate pressure p_3^* which is the inlet pressure of TW as

$$p_3^* = p_4 \left[1 - r_T \left(\left(\frac{p_3}{p_4} \right)^{-\left(\frac{k_g - 1}{k_g} \right)} - 1 \right) \right]^{\frac{-k_g}{k_g - 1}} = 2.6395 \times 10^5 Pa \quad \text{---------- (3.7)}$$

Now, the pressure force acting on the inlet surface of the turbine $F_{1,T}$ can be calculated for the given value of inlet diameter of the turbine from reference [30] $D_3 = 29.6mm$ as

$$F_{1,T} = A_3 p_3^* = \frac{\pi D_3^2}{4} p_3^* = 181.6305N \quad \text{---------- (3.8)}$$

From the reference [30] for the given value of blade height at inlet $b_3 = 0.709mm$ and at outlet $b_4 = 4.45mm$ of the TW one can calculate the mean blade height as

$$b_{m,T} = \frac{b_3 + b_4}{2} = 2.5795mm = 2.5795 \times 10^{-3} m$$

Therefore the projected area in the axial direction (here along x-direction) of the shroud surface $A_{S,T}$ for given value of the tip and hub diameter of the turbine $D_{tip} = 17.8mm = 17.8 \times 10^{-3} m$, $D_{hub} = 8.9mm = 8.9 \times 10^{-3} m$ number of blades $z = 10$, and thickness of the blade $t = 0.6mm = 0.6 \times 10^{-3} m$ from the reference [30], can be calculated as

$$A_{S,T} = \frac{\pi \left(D_{tip}^2 - D_{hub}^2 \right)}{4} - z \times b_{m,T} \times t = 5.3268 \times 10^{-4} m^2$$

The mean pressure of the turbine wheel on the basis of inlet pressure p_3^* and the outlet pressure p_4 can be calculated as

$$p_{m,T} = \left(\frac{p_3^* + p_4}{2} \right) = 1.9197 \times 10^5 Pa$$

By using the mean pressure $p_{m,T}$, of the inlet and outlet pressure of the TW, the pressure force $F_{2,T}$ can be calculated as

$$F_{2,T} = A_{S,T}\, p_{m,T} = A_{S,T}\left(\frac{p_3^* + p_4}{2}\right) = 102.2606N \qquad \text{---------- (3.9)}$$

Where

$A_{S,T}$ is the projected area in the axial direction (here along x-direction) of the shroud surface

p_3^* is the inlet pressure of the TW

p_4 is the outlet pressure of the TW.

For the reference [30] inlet pressure p_3^*, inlet temperature $T_3 = 104.57K$ and inlet density $\rho_{in,T} = 7.175kgm^{-3}$ the mass flow rate $\dot{m}_T$ can be calculated as

$$\dot{m}_T = \rho_{in,T} \times A_3\left(\frac{\pi \times D_3 \times N}{60}\right) = 0.765kgm^{-3}$$

Where

N is the RPM of the TW.

For the given value of the RPM of TW, say N =100000rpm.

The impulsive force $F_{3,C}$ can be calculated by using the momentum theorem and the perfect gas equation as follows

$$F_{3,T} = \dot{m}_T\, C_{m,3} = \dot{m}_T\left(\frac{\dot{m}_T}{\rho_{in,T} A_3}\right) = \frac{\dot{m}_T^{\,2} R_a T_3}{p_3^* A_3} = 96.7741N \qquad \text{---------- (3.10)}$$

Where

$\dot{m}_T$ is the mas flow rate of air through TW;

$C_{m,3}$ is the meridional component of the air velocity at turbine inlet;

R_a is the air characteristic gas constant (i.e., $R_a = 287.058Jkg^{-1}K^{-1}$);

T_3 is the TW inlet air temperature;

p_3^* is pressure of the TW at inlet;

And A_3 is the TW cross-sectional area at inlet.

According to the CFD result if the gap between bearing bushing and the back face of TW is more than 1mm then the pressure at the back face of TW is nearly remain unchanged. Hence, the pressure force $F_{4,T}$ corresponding to the pressure p_4 can be calculated as

$$F_{4,T} = A_{bf,T} p_3 = A_3 p_3 = 181.6305N \quad \text{---------- (3.11)}$$

Where

$A_{bf,T}$ is the back face surface area of the TW;

p_3 is the inlet pressure of the TW.

The resulting force acting on the TW can be calculated as

$$F_{TW} = -F_{1,T} - F_{2,T} - F_{3,T} + F_{4,T} = -199.0347N \quad \text{---------- (3.12)}$$

Hence the resultant force acting on the rotor is

$$F_{T,ax} = F_{CW} + F_{TW} = -132.1739N \quad \text{---------- (3.13)}$$

Here –ve sign shows that the direction of the resultant thrust load is from turbine to compressor side.

3.2 Variation of Axial Load w.r.t RPM of Rotor

By using the above mathematical calculation the variation of Axial-load with RPM is shown in Fig.3.2.

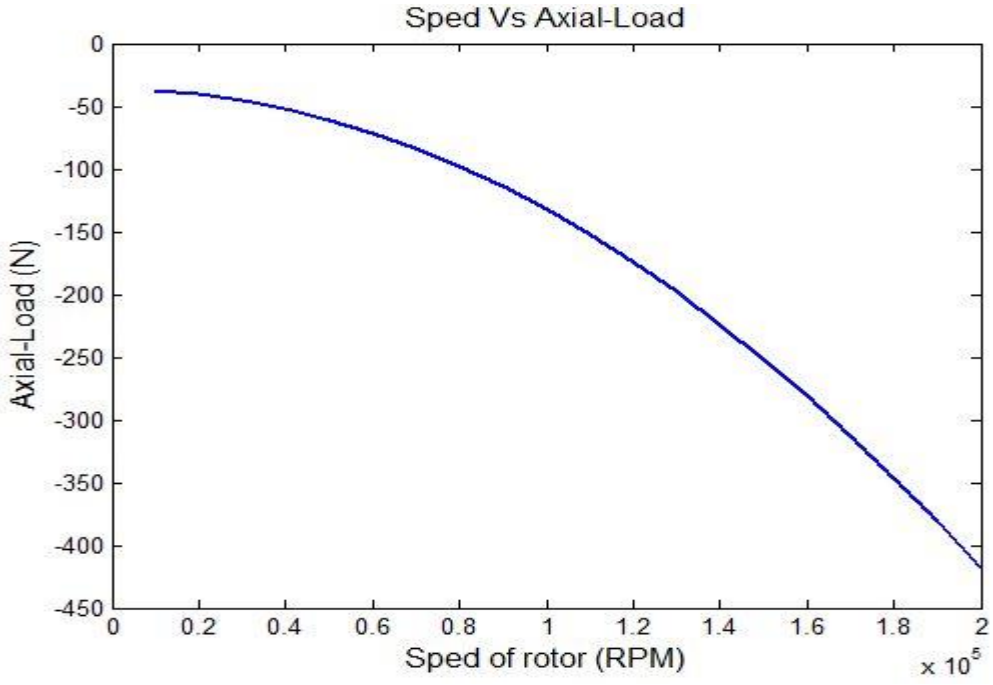

Figure 3.0:2: Axial-load Vs RPM

From the above graph it is clear that the load carrying capacity of the designed turbocharger at the 1e5 rpm is 145.75 N. As our aim is to design the bearing which can sustain the thrust load generated by the rotor at an rpm of 1e5. Therefore, now our aim is to designed a bearing which can sustain at least 145.75 N or more than that.

Chapter-4

Mathematical Formulation

4.1 Assumptions of Reynolds Equation

Generalised fluid equation for simple gas thrust bearing is the simplified general fluid mechanics equations. Here we will use the Continuity equation, Navier-Stokes equation and energy equations in order to derive the generalised fluid equation for simple gas thrust bearing. Differential equation for the aerodynamic bearing was derived by ***Osborne Reynold*.** The mechanism of lubrication through the generation of a viscous liquid film between the moving surfaces is explained by Reynolds. For the occurrence of aerodynamic lubrication conditions are required:-

a. The relative motion is required between the two surfaces so that the lubricating film can carry the load.
b. There should be some inclination between the surfaces.

Assumptions of the Reynolds equation:

1. Newton's law of viscosity is followed by the lubricant.
2. The air film inertia forces are negligible.
3. The lubricant viscosity is constant.
4. The film curvature effect is neglected with respect to film thickness. The film is assumed too thin so that the pressure is assumed to be constant across the film thickness.
5. Continuous supply of lubricant takes place.
6. There is no any boundary slip.
7. The shaft and bearing are assumed to be rigid.

4.2 Governing Equation

By considering gas flow as isothermal, isoviscous, laminar and ideal, the lubricating behaviour of the gas can be assumed to be governed by the Reynolds equation. The Reynolds equation in Cartesian form for the compressible fluid can be written as

$$\frac{\partial}{\partial x}\left(\frac{ph^3}{12\mu}\frac{\partial p}{\partial x}\right)+\frac{\partial}{\partial y}\left(\frac{ph^3}{12\mu}\frac{\partial p}{\partial y}\right)=\frac{1}{2}U\frac{\partial(ph)}{\partial x} \qquad \text{---------- (4.1)}$$

The above Cartesian form of Reynolds equation can be written in Polar coordinates (in θ-R plane) as:

$$\frac{1}{r}\frac{\partial}{\partial\theta}\left(ph^3\frac{\partial p}{\partial\theta}\right)+\frac{\partial}{\partial r}\left(ph^3 r\frac{\partial p}{\partial r}\right)=6\mu\omega r\frac{\partial}{\partial\theta}(ph) \qquad \text{---------- (4.2)}$$

Introducing the non-dimensional variables.

$$H=\frac{h}{h_l};\ R=\frac{r}{r_i};P=\frac{p}{p_{at}}$$

The above equation we can get the non-dimensional form of the Reynolds equation becomes

$$\frac{1}{R}\frac{\partial}{\partial\theta}\left(PH^3\frac{\partial P}{\partial\theta}\right)+\frac{\partial}{\partial R}\left(PH^3R\frac{\partial P}{\partial R}\right)=\wedge R\frac{\partial}{\partial\theta}(PH) \qquad \text{---------- (4.3)}$$

Where

$$\wedge=\frac{6\mu\omega}{p_{at}}(\frac{r_i}{h_l})^2$$

As we know $P\frac{\partial P}{\partial\theta}=\frac{1}{2}\frac{\partial P^2}{\partial\theta}$, Eq. 3.3 modifies as

$$\frac{1}{2R}\frac{\partial}{\partial\theta}\left(H^3\frac{\partial P^2}{\partial\theta}\right)+\frac{1}{2}\frac{\partial}{\partial R}\left(H^3R\frac{\partial P^2}{\partial R}\right)=\wedge R\frac{\partial}{\partial\theta}(PH)$$

$$\Rightarrow\frac{1}{R}\frac{\partial}{\partial\theta}\left(H^3\frac{\partial P^2}{\partial\theta}\right)+\frac{\partial}{\partial R}\left(H^3R\frac{\partial P^2}{\partial R}\right)=2\wedge R\frac{\partial}{\partial\theta}(PH) \qquad \text{---------- (4.4)}$$

Equation (2.14) can be expressed as

$$A+B+C=0 \qquad \text{---------- (4.5)}$$

Where

$$A=\frac{1}{R}\frac{\partial}{\partial\theta}(\mathrm{H}^3\frac{\partial \mathrm{P}^2}{\partial\theta}) \qquad \text{---------- (4.6)}$$

$$B = R\left(\frac{\partial}{\partial R}\left(H^3\frac{\partial P^2}{\partial R}\right)\right) \qquad \text{---------- (4.7)}$$

$$C = -2 \wedge R\frac{\partial(\mathrm{PH})}{\partial\theta} \qquad \text{---------- (4.8)}$$

4.3 Numerical Method

There are several methods in engineering and computational fluid dynamics to solve the Partial Differential Equations like Reynolds equation. Some of them are Finite Element Method, Finite Volume Method, and Finite Difference Method etc. Among all these mentioned methods the Finite Difference Method is very popular for simple problems due to its easy implementation and understanding. Therefore, here we are following the FDM to solve the above differential form of the Reynolds equation to discretise it into a linear equation. Finite difference Method is of three types: -

a. **Forward Finite Difference Method**
b. **Backward Finite Difference Method and**
c. **Central Finite Difference Method**

Here we are following the Central FDM the detail of which can be explained as follows.

The Taylor series can be utilised as follows

$$p(x+\Delta x) = p(x)+(\Delta x)\frac{\partial p}{\partial x}+\frac{1}{2}(\Delta x)^2\frac{\partial^2 p}{\partial x^2}+\ldots \qquad \text{---------- (4.9)}$$

$$p(x-\Delta x) = p(x)-(\Delta x)\frac{\partial p}{\partial x}+\frac{1}{2}(\Delta x)^2\frac{\partial^2 p}{\partial x^2}-\ldots \qquad \text{---------- (4.10)}$$

By subtracting Eq. 4.9 from Eq. 4.8 we get

$$p(x+\Delta x)-p(x-\Delta x) = 2\Delta x\frac{\partial p}{\partial x}$$

$$\Rightarrow \frac{\partial p}{\partial x} = \frac{p(x+\Delta x)-p(x-\Delta x)}{2\Delta x} \qquad \text{---------- (4.11)}$$

In the same way one can write the above equation for $p_{i,j}$ as follows

$$\frac{\partial P_{i,j}^2}{\partial\theta} = \frac{P_{i+1,j}^2 - P_{i-1,j}^2}{2\Delta\theta} \qquad \text{---------- (4.12)}$$

and $$\frac{\partial}{\partial\theta}\left(\frac{\partial P_{i,j}^2}{\partial\theta}\right)=\frac{\left(\frac{\partial P^2}{\partial\theta}\right)_{i+0.5,j}-\left(\frac{\partial P^2}{\partial\theta}\right)_{i-0.5,j}}{\Delta\theta}$$ ---------- (4.13)

Using Eq. 4-11 in Eq. 4.12 we gets

$$\frac{\partial}{\partial\theta}\left(\frac{\partial P_{i,j}^2}{\partial\theta}\right)=\frac{P_{i+1,j}^2-2P_{i,j}^2+P_{i-1,j}^2}{\left(\Delta\theta\right)^2}$$ ---------- (4.14)

By using the above kind of approximation we can write

$$\frac{\partial}{\partial\theta}(\mathrm{H}^3\frac{\partial \mathrm{P}^2}{\partial\theta})=\left(\frac{H_{i,j+0.5}^3P_{i,j+1}^2-\left(H_{i,j+0.5}^3+H_{i,j-0.5}^3\right)P_{i,j}^2+H_{i,j-0.5}^3P_{i,j-1}^2}{\left(\Delta\theta\right)^2}\right)$$

$$\frac{\partial}{\partial R}\left(H^3\frac{\partial P^2}{\partial R}\right)=\left(\frac{H_{i+0.5,j}^3P_{i+1,j}^2-\left(H_{i-0.5,j}^3+H_{i+0.5,j}^3\right)P_{i,j}^2+H_{i-0.5,j}^3P_{i-1,j}^2}{\left(\Delta R\right)^2}\right)$$

Where

$$H_{i+0.5,j}=\frac{H_{i+1,j}+H_{i,j}}{2}$$

$$H_{i-0.5,j}=\frac{H_{i,j}+H_{i-1,j}}{2}$$

$$H_{i,j+0.5}=\frac{H_{i,j}+H_{i,j+1}}{2}$$

$$H_{i,j-0.5}=\frac{H_{i,j}+H_{i,j-1}}{2}$$

Where

$$A=\frac{1}{R}\frac{\partial}{\partial\theta}(\mathrm{H}^3\frac{\partial \mathrm{P}^2}{\partial\theta})$$

$$=\frac{1}{R}\left(\frac{H_{i,j+0.5}^3P_{i,j+1}^2-\left(H_{i,j+0.5}^3+H_{i,j-0.5}^3\right)P_{i,j}^2+H_{i,j-0.5}^3P_{i,j-1}^2}{\left(\Delta\theta\right)^2}\right)$$ ---------- (4.15)

$$B=R\left(\frac{\partial}{\partial R}\left(H^3\frac{\partial P^2}{\partial R}\right)\right)$$

$$= R\left(\frac{H^3_{i+0.5,j} P^2_{i+1,j} - \left(H^3_{i-0.5,j} + H^3_{i+0.5,j} \right) P^2_{i,j} + H^3_{i-0.5,j} P^2_{i-1,j}}{\left(\Delta R \right)^2} \right) \quad \text{---------- (4.16)}$$

$$C = -2 \wedge R \frac{\partial (\mathrm{PH})}{\partial \theta}$$

$$= -2 \wedge R\left(\frac{P_{i,j+1} H_{i,j+1} - P_{i,j-1} H_{i,j-1}}{\Delta \theta} \right) \quad \text{---------- (4.17)}$$

Equation (3.4) can be discretized by applying the Central-Finite Difference Method (FDM) and after discretisation and some rearrangement the equation (3.4) can be expressed as

$$P^2_{i,j} = \left(\frac{k_1}{k} \right) P^2_{i+1,j} + \left(\frac{k_2}{k} \right) P^2_{i-1,j} + \left(\frac{k_3}{k} \right) P^2_{i,j+1} + \left(\frac{k_4}{k} \right) P^2_{i,j-1} + \left(\frac{k_5}{k} \right) P_{i,j+1} + \left(\frac{k_6}{k} \right) P_{i,j-1} \quad \text{---------- (4.18)}$$

If we put $\overline{p} = P^2$, the above equation can be expressed as

$$\overline{p}_{i,j} = \left(\frac{k_1}{k} \right) \overline{p}_{i+1,j} + \left(\frac{k_2}{k} \right) \overline{p}_{i-1,j} + \left(\frac{k_3}{k} \right) \overline{p}_{i,j+1} + \left(\frac{k_4}{k} \right) \overline{p}_{i,j-1} + \left(\frac{k_5}{k} \right) \sqrt{\overline{p}_{i,j+1}} + \left(\frac{k_6}{k} \right) \sqrt{\overline{p}_{i,j-1}} \quad \text{- (4.19)}$$

Where

$$k = \left(\frac{H^3_{i,j+0.5} + H^3_{i,j-0.5}}{R\left(\Delta \theta \right)^2} \right) + \left(\frac{R\left(H^3_{i-0.5,j} + H^3_{i+0.5,j} \right)}{\left(\Delta R \right)^2} \right)$$

$$k1 = \frac{R}{\left(\Delta R \right)^2} H^3_{i+0.5,j} + \frac{1}{2\left(\Delta R \right)} H^3_{i,j}$$

$$k2 = \frac{R}{\left(\Delta R \right)^2} H^3_{i-0.5,j} - \frac{1}{2\left(\Delta R \right)} H^3_{i,j}$$

$$k3 = \frac{1}{R\left(\Delta \theta \right)^2} H^3_{i,j+0.5}$$

$$k4 = \frac{1}{R\left(\Delta \theta \right)^2} H^3_{i,j-0.5}$$

$$k5 = -\left(\frac{2 \wedge R}{\Delta \theta} \right) H_{i,j+1}$$

$$k6 = \left(\frac{2 \wedge R}{\Delta \theta} \right) H_{i,j-1}$$

Now we will go for the MATLAB programming to generate the pressure profile. Flow chart for the MATLAB coding is shown in figure below.

4.4 Flow Chart

All the steps followed in order to find the static parameters like pressure profile and load carrying capacity for the air thrust bearing using MATLAB code can be shown through a floe chart as follows .

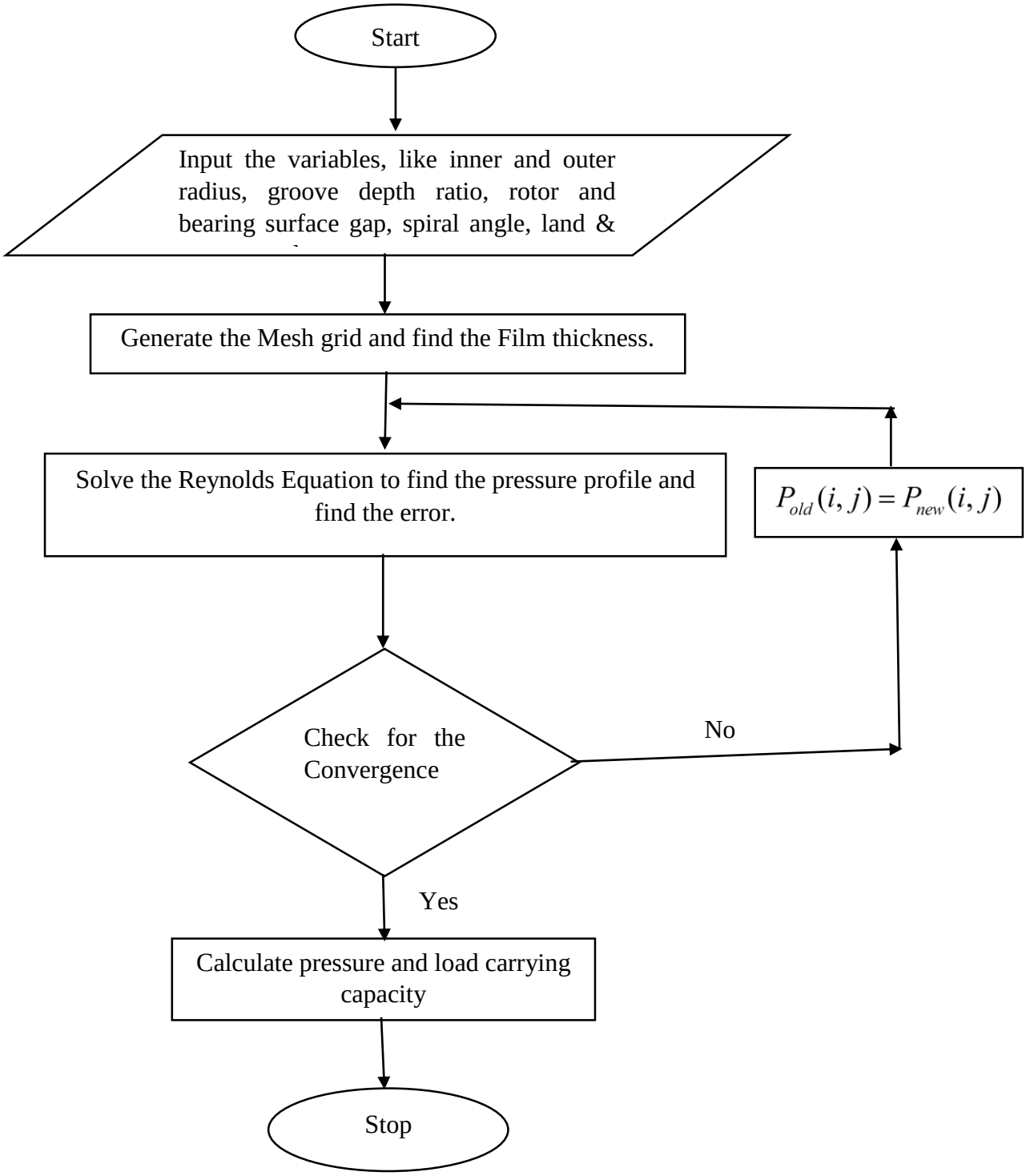

Chapter-5

Results and Discussion

Current work is an effort to understand different parameters and its effects on the performance of gas lubricated bearing by analysing it theoretically and graphically. This paper explains the static parameters like pressure distribution and load carrying capacity of gas lubricated spiral grooved thrust bearing. An attempt is done for optimization of the bearing performance. All these calculations are done with respect to different input parameters like inner and outer radius, no of grooves, rpm, groove angle, land angle, spiral angle, inner to outer radius ratio, groove depth ratio, clearance between the rotor and the bearing surface etc. Here we have designed two types of spiral bearings

a. **Siple Spiral grooved bearing**
b. **Spiral & Deverging grooved bearing**

5.1 Siple Spiral grooved bearing

5.1.1 Design of Spiral grooves

Logarithmic spiral grooves were designed over the bearing surface and shown in Fig.-

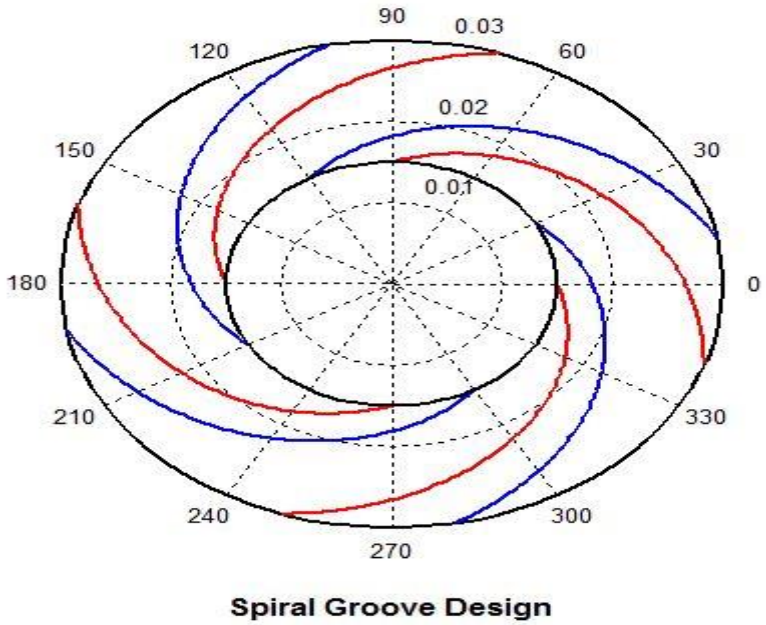

Figure 5:0:1 Spiral Groove Design

Figure 5.1:

5.1.2 Film Thickness

MATLAB coding is done to calculate the film thickness for the optimized no of grooves as shown below.

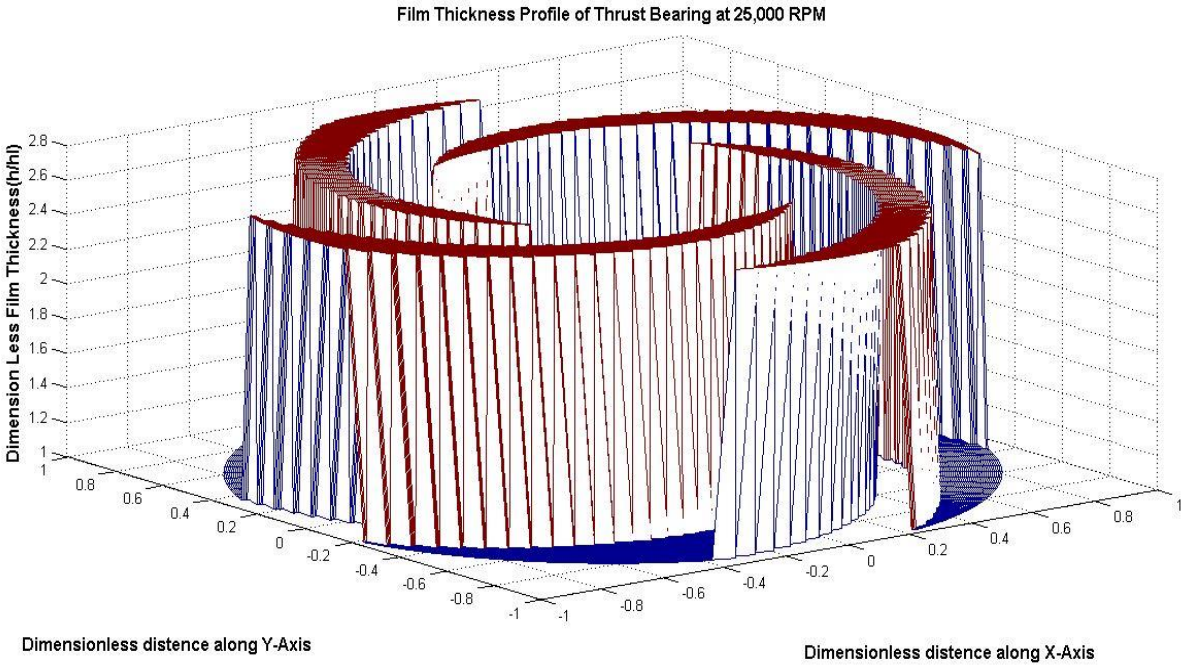

Figure 5:0:2 Film Thickness

5.1.3 Pressure Profile

Because of the shearing action between fluid and bearing surface pressure generates. At the same time due to the variation of the film thickness between the groove and pad, pressure variation takes place. This pressure variation can be discretised the differential form of the Reynolds equation by Finite Difference Method. Now the linear form of the equation is coded with MATLAB and the generated pressure profile is shown below.

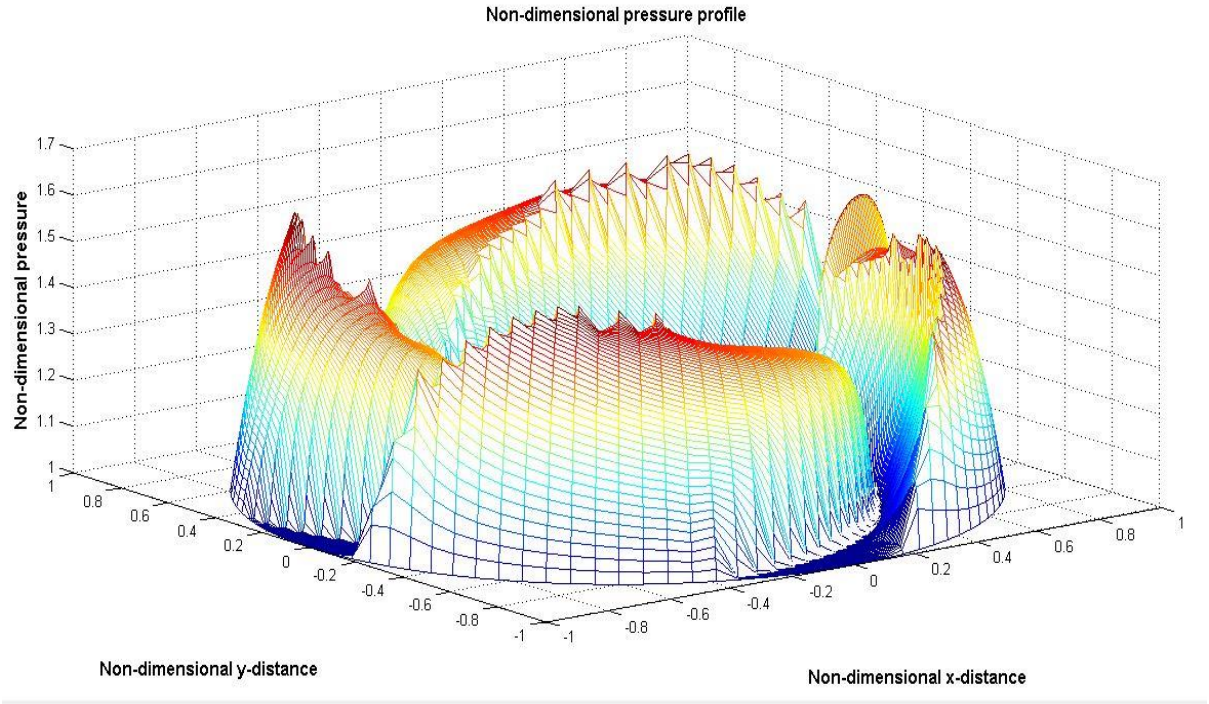

Figure 5:0:3 Pressure profile of spiral groove

5.1.4 Speed Vs Non-dimensional Load Carrying capacity

The Non-dimensional load carrying capacity at different speeds ware drawn and their variation is shown in Fig.5.4.

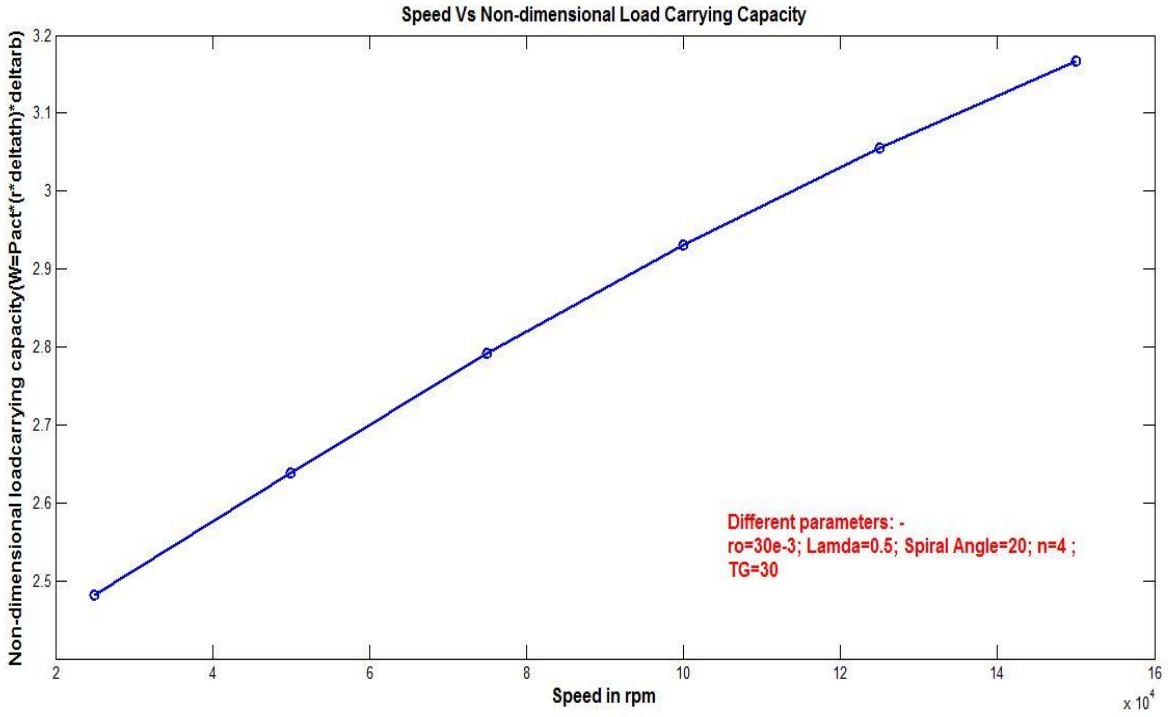

Figure 5:0:4 Speed Vs Non-dimensional Load

The above graph shows that for given value of design input parameters with increase of speed the non-dimensional load carrying capacity of the designed bearing increases.

5.1.5 Optimization of the Design

5.1.5.1 Graph between No. of grooves Vs Non-dimensional Load:- In order to optimize the design we have finded out the number of grooves which can take the maximum load for the given design parameters. For this purpose we have drawn the graph between number of grooves Vs load carrying capacity and we find the variation as shown in Fig.5.5.

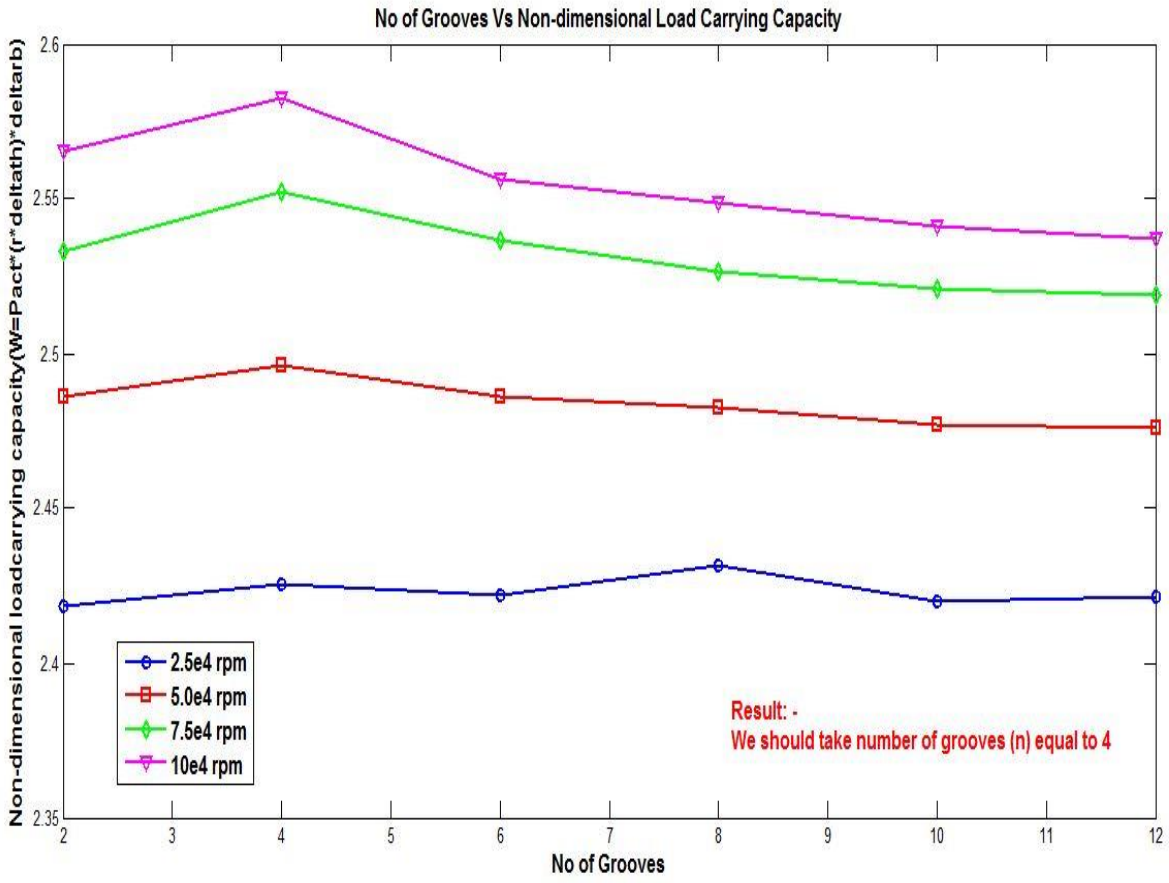

Figure 5:0:5 No. of Grooves Vs Non-dimensional Load

The above graph shows that if we take four number of grooves then we can get the maximum load carrying capacity. Therefore we desided to take four number of grooves for our design.

5.1.5.2 Graph between L vs Nin-dimensional Load: - A graph between L, the inner and outer diameter ratio, and Non-dimensional load carrying capacity, at different speed, is draown which shows the variation between them as shown in Fig. 5.6.

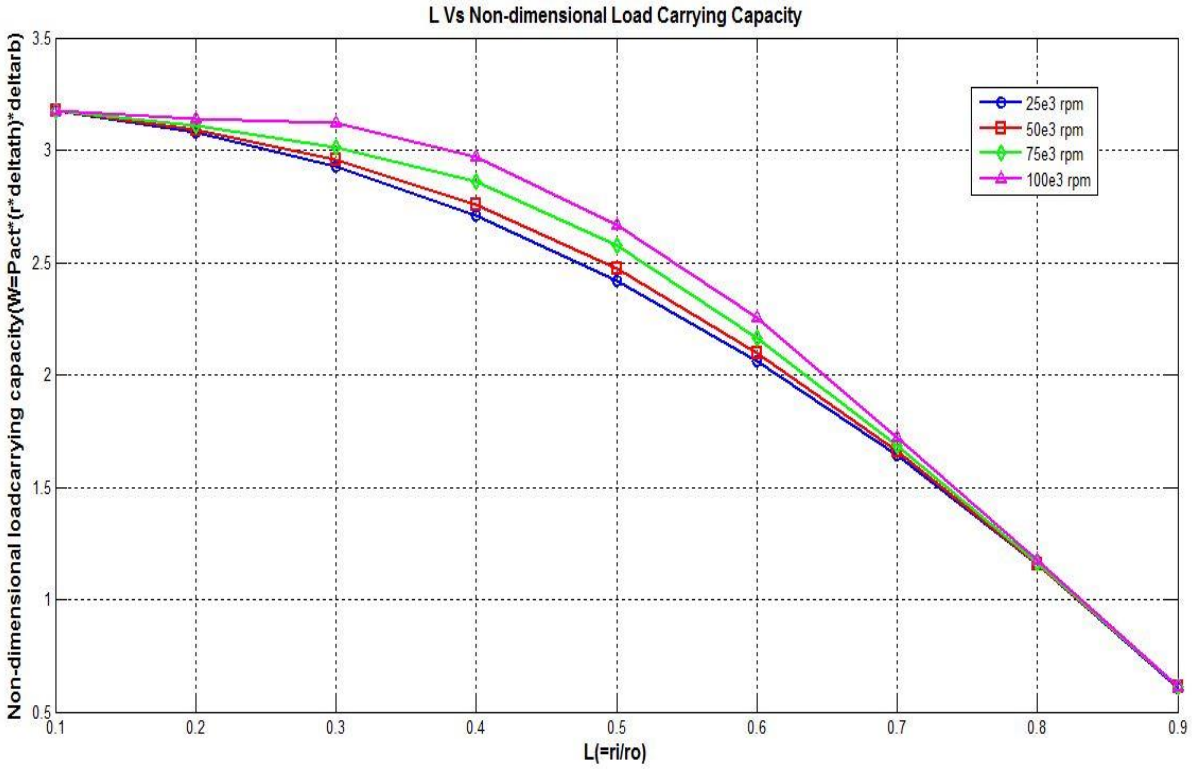

Figure 5:0:6 L Vs Non-dimensional Load

The above figure shows that at all rpm the non-dimensional load is maximum when we take L as 0.1, but at this ratio the outer radius will become ten times more than the inner radius which brings the stability problem of the rotor. Therefore we have selected L as 0.5 for our design.

5.2 Spiral & Deverging grooved bearing

5.2.1 Design of spiral and diverging curve

The Spiral and diverging grooves were designed with the help of MATLAB coding and the designed bearing is shown in Fig.5.7.

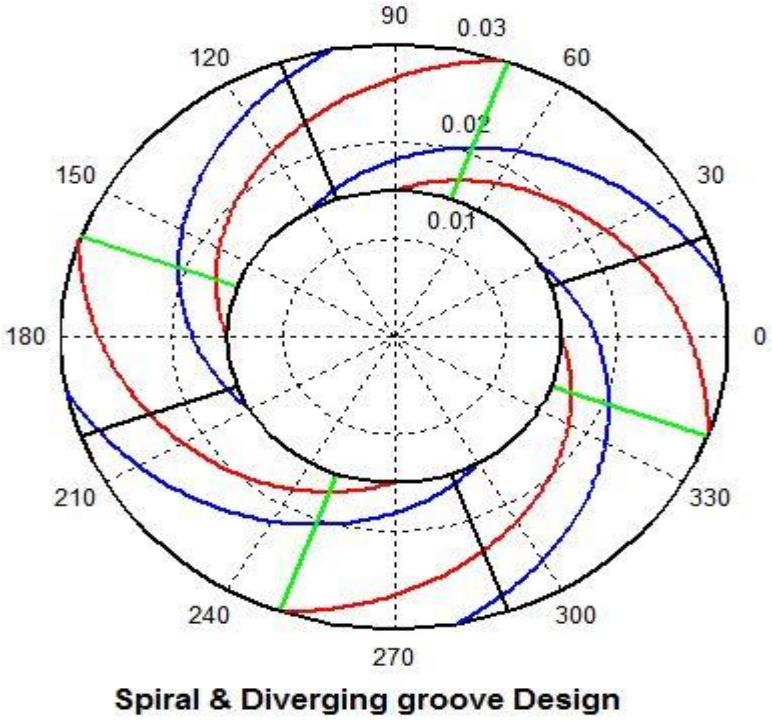

Figure5:0:7 Spiral and Diverging Grooves Design

5.2.2 Film Thickness

For the above designed curves and the optimum designed input parameters the film thickness coding is done and the result is shown in Fig 5.8.

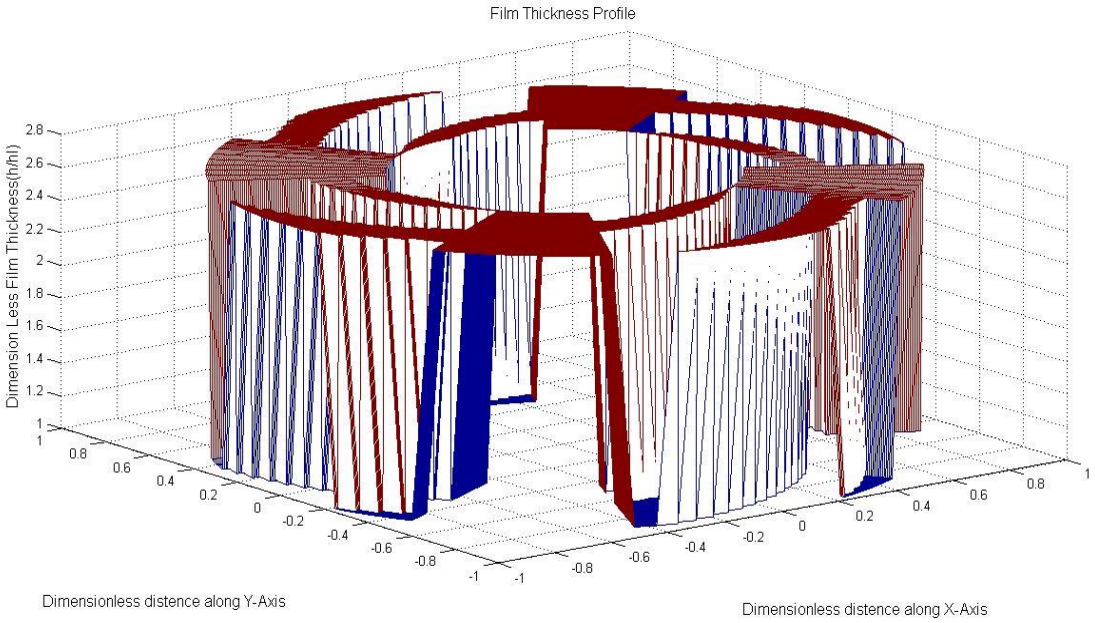

Figure 5:0:8 Combine film thickness

In the above figure we have taken non-dimensional value of distances along X- and Y-axes and along Z-axis direction we got the non-dimensional pressure.

5.2.3 Pressure Profile

The pressure profile for the designed bearing is obtained in Fig.5.9. Here we have converted the pressure into a non-dimensional quantity during mathematical modelling so that we can handle it without any dimensional handling problem.

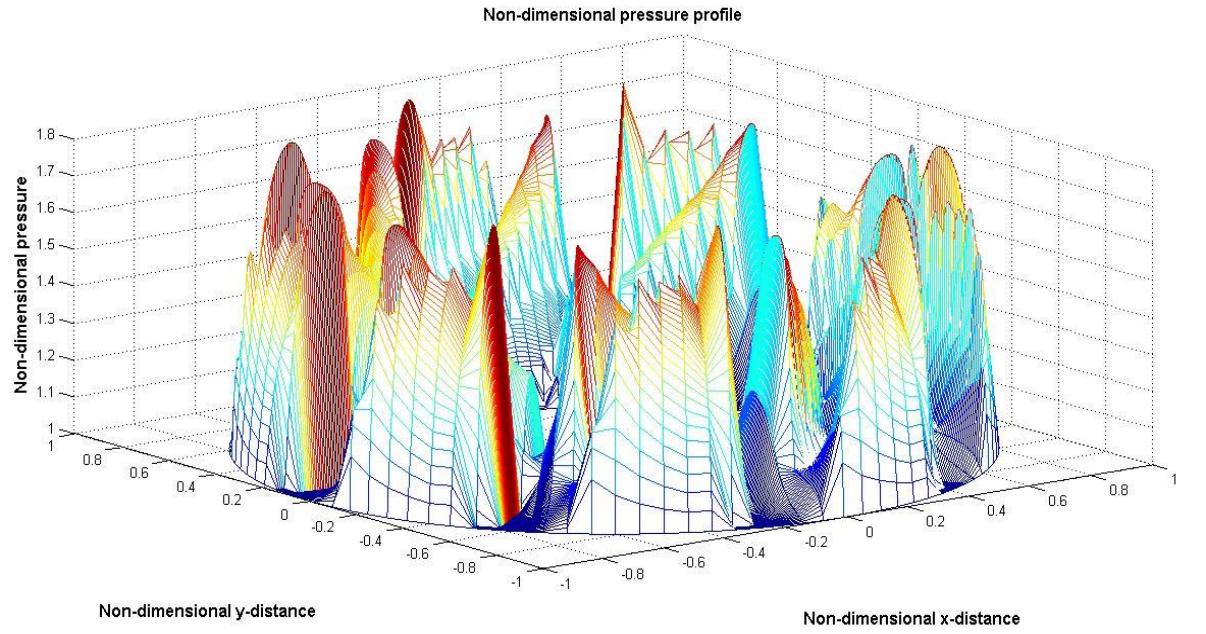

Figure5:0:9 Combine Pressure profile

5.2.4 Speed Vs Non-dimensional load

To know the effect of speed on the non-dimensional load carrying capacity of the designed bearing we have drawn the graph between speed and non-dimensional load and their variation is shown in Fig.5.10.

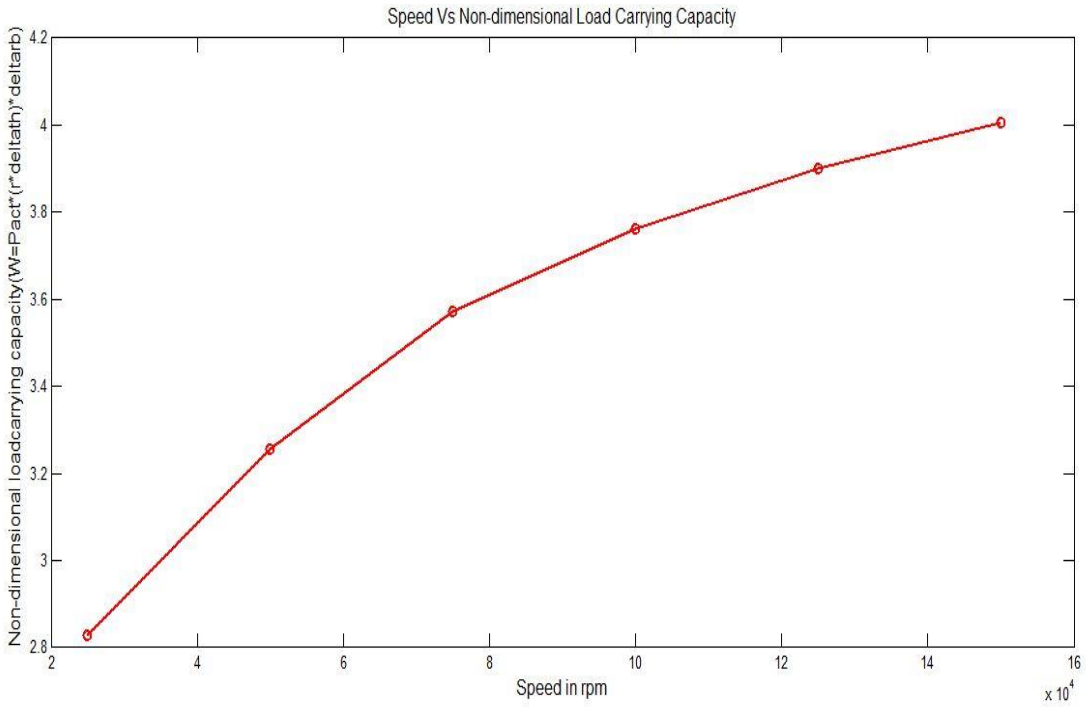

Figure 5:0:10 Combine Speed Vs Non-dimensional load

From the above diagram we find that the non-dimensional load carrying capacity of the designed bearing increases with speed.

5.2.5 Speed Vs Actual Load

The actual load carrying capacity of the designed bearing can be shown by this graph. This variation is shown in Fig.5.11.

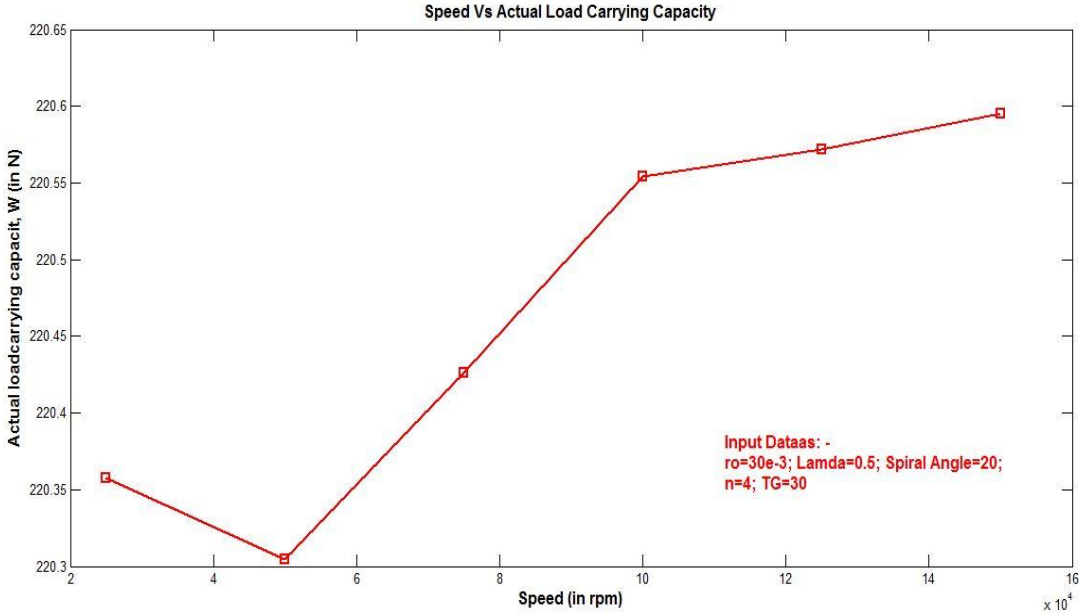

Figure 5:11 Combine Speed Vs Actual Load

The above graph shows that there is some decrement in the actual load carrying capacity of the designed bearing up to 50000 rpm and there is sharp increment in load carrying capacity from 5e4 rpm to 1e5 rpm. After that the increment rate of the actual load carrying capacity becomes low but it increases continuously.

Chapter-6

Conclusion and Future Work

6.1 Conclusion

The thrust load is calculated from the designed turbocharger [30]. To sustain the above thrust load two types of bearings were designed

I. Spiral grooved thrust bearing.
II. Spiral and Diverging groove thrust bearing.

After design and optimization following conclusions were drawn.

Maximum load carrying capacity of the designed Spiral Grooved bearing for designated bearing dimension is 222.6N, which is sufficient to take the generated axial thrust load of the designed turbocharger. On the other hand Maximum load carrying capacity of the designed Spiral & Diverging Grooved bearing is 220.42N, which is also sufficient to take the generated axial thrust load of the designed turbocharger. The load carrying capacity of both the bearings are very near to each other. Therefore, it is concluded that only the spiral groove is sufficient to carry the generated axial thrust load.

6.2 Future Scope

- Improvement in the design of Diverging Grooved bearing can be done.
- Transient analysis of both types of bearing can be done.
- Fabrication and testing of the designed bearing is to be done for the turboexpander used in our nitrogen plant.

References: -

1. Whipple, R. T. P. (1949). Herringbone Pattern Thrust Bearing, AERE T/M 29.
2. Muijderman, E. A. (1965). New Possibilities for the Solution of Journal Bearing Problems by Mean of Spiral Groove Principle. *Proc. Inst. of Mech. Eng, 1966*, 75.
3. Vohr, J. H., & Chow, C. Y. (1965). Characteristics of herringbone-grooved, gas-lubricated journal bearings. *Journal of Basic Engineering*, *87*(3), 568-576.
4. Hirs, G. G. (1965). The load capacity and stability characteristics of hydrodynamic grooved journal bearings. *ASLE transactions*, *8*(3), 296-305.
5. Bootsma, J. (1973). The gas liquid interface and the load capacity of helical grooved journal bearings. *Journal of Lubrication Technology*, *95*(1), 94-100.
6. Smalley, A. J. (1972). The narrow groove theory of spiral grooved gas bearings: Development and application of a generalized formulation for numerical solution. *Journal of Lubrication Technology*, *94*(1), 86-92.
7. Reinhoudt, J. P. (1972). *On the stability of rotor-and-bearing systems and on the calculation of sliding bearings* (Doctoral dissertation, Philips Research Laboratories).
8. Yavelov, I. S. (1983). On the Influence of Spiral Groove Depth on the Experimental Characteristic of Radial Hydrodynamic Bearings, Trenic Iznos Vol. 4, No. 1, pp. 134-146.
9. Cunning, R. E. and Fleming, D. P. (1965) *Experimental Stability Studies of the Herringbone Grooved Gas Lubricated Journal Bearing*, Trans. ASME, Journal of Lubrications Technology.
10. Malanski, S. B. (1967). Experiments on an Ultrastable Gas Journal bearing. *Journal of Lubrication Technology*, *89*(4), 433-438.
11. Molyneaux, A. K., & Leonhard, M. (1989). The Use of Spiral Groove Gas Bearings in a 350 000 rpm Cryogenic Expander. *Tribology transactions*, *32*(2), 197-204.
12. Dewar, D. M. (1974). An Analysis of Grease and Oil Lubricated Spiral Grooved Bearings. *Journal of Lubrication Technology*, *96*(2), 275-283.
13. Muijderman, E. A. (1979). Grease-lubricated spiral groove bearings. *TRIBOLOGY international*, *12*(3), 131-137.

14. Fedrick, T, et al. (1967). *Operation of Hydrodynamic Journal Bearings in Sodium at a Temperatureo of 800 ^{0}F*. NationalA eronatuica nd SpaceA dministration, Lewis ResearchC entreC levelandO hio.
15. Vohr, J. H., & Chow, C. Y. (1969). Theoretical analysis of spiral-grooved screw seal for turbulent operation. *Journal of Lubrication Technology*, *91*(4), 675-686.
16. Bootsma,J . (1964). *The Effects of Viscosity Variation with Temperatureo n the Performance of Spiral Groove Thrust Bearings*. ASLE Transactions.
17. Yavelov, I. S., (1987*). Characteristics of Loaded Hydrodynamic Journal Bearing Spiral Grooves*, Soviet Journal of Fiction and Wear, Vol. 8, Part No. 3.
18. Nobuyoshi, K., Yasumi Ozawa Shuji Kamaya and Mutaka Miyake (1989). *Static Characteristics of the Regular and Reversible Rotation type Herringbone Grooved Journal bearing*, Trans. ASME, Journal of Tribology, Vol. 11, pp. 484-490.
19. Hirs, G. G., & Sonneveld, J. I. (1980). A New Method for Etching Surfaces of Bearings and Other Machine Elements. *J. Lubric. Technol. (Trans. ASME)*, *102*(3), 395-399.
20. Huang, Y., & Chen, D. G. (1996). Effects of partial-grooving on the performance of spiral groove bearings: analysis using a perturbation method. *Tribology international*, *29*(4), 281-290.
21. Ren, L., & Xiaoli, W. (2011, February). Dynamic characteristics analysis of micro air spiral grooved thrust bearing-rotor system. In *Nano/Micro Engineered and Molecular Systems (NEMS), 2011 IEEE International Conference on* (pp. 719-723). IEEE.
22. Liu, R., Wang, X. L., & Zhang, X. Q. (2012). Effects of gas rarefaction on dynamic characteristics of micro spiral-grooved thrust bearing. *Journal of tribology*, *134*(2), 022201.
23. Huang, J. B., Tong, Q. Y., & Mao, P. S. (1992). Gas-lubricated microbearings for microactuators. *Sensors and Actuators A: Physical*, *35*(1), 69-75.
24. Wong, C. W., Zhang, X., Jacobson, S. A., & Epstein, A. H. (2004). A self-acting gas thrust bearing for high-speed micro-rotors. *Micro-electromechanical Systems, Journal of*, *13*(2), 158-164.
25. Grigor'ev, B. S., & Smirnov, D. B. (2013). Calculation of static characteristics of spiral-grooved thrust bearings over a wide compressibility range. *Journal of Machinery Manufacture and Reliability*, *42*(3), 236-239.
26. Wang, B., Zhang, H., & Cao, H. (2013). Flow dynamics of a spiral-groove dry-gas seal. *Chinese Journal of Mechanical Engineering*, *26*(1), 78-84.

27. Šimek, J., & Lindovský, P. (2014). Development of aerodynamic bearing support for application in air cycle machines.
28. Villavicencio, R., Colombo, F., Raparelli, T., & Viktorov, V. (2013). Development of dynamic gas thrust bearings: design and first experimental results.
29. Khan M.Z., Performance studies of oil lubricated helical groove journal bearing. Thesis Submitted for the Degree of Doctor of Philosophy, Department of Mechanical Engineering Brunel, The University of West London May 1992.
30. Hung Ping., Numerical Calculation of Lubrication, methods and Programs. Singapore, John Wiley, 2013.